Synthesis of high-surface area transition metal sponges and their catalytic properties

Journal:	*New Journal of Chemistry*
Manuscript ID	NJ-ART-04-2019-002096.R1
Article Type:	Paper
Date Submitted by the Author:	22-May-2019
Complete List of Authors:	Islam, Md; University of Texas at EL Paso, Chemistry Rosales, Jose; University of Texas at EL Paso, Chemistry Ricardo, Saenz Arana; University of Texas at EL Paso, Chemistry Arrieta, Roy; The University of Texas at El Paso Kim, Hoejin; University of Texas at EL Paso, Chemistry Sultana, Kazi; University of Texas at EL Paso, Chemistry Lin, Yirong; University of Texas at El Paso, Department of Mechanical Engineering Villagran, Dino; University of Texas at El Paso, Department of Chemistry Noveron, Juan; University of Texas at El Paso, Chemistry

Synthesis of high-surface area transition metal sponges and their catalytic properties

Md. Tariqul Islam,[ab] Jose Rosales,[a] Ricardo Saenz-Arana,[a] Roy Arrieta,[a] Hoejin Kim,[c] Kazi Afroza Sultana,[d] Yirong Lin,[c] Dino Villagran,[ab] Juan C. Noveron.[ab*]*

[a] Department of Chemistry, University of Texas at El Paso, 500 West University Avenue, El Paso, Texas 79968, USA.

[b] Nanosystems Engineering Research Center for Nanotechnology-Enabled Water Treatment, 6100 Main St, Houston, TX 77005, USA.

[c] Department of Mechanical Engineering, University of Texas at El Paso, 500 West University Avenue, El Paso, Texas 79968, USA.

[d] Department of Environmental Science and Engineering, University of Texas at El Paso, 500 West University Avenue, El Paso, Texas 79968, USA.

Keywords: Metal sponges, Catalysis, Reduction, 4-nitrophenol, Methyl orange, Methylene blue.

Abstract

Sucrose mediated facile route for the preparation of high-surface area cobalt (Co), nickel (Ni), and copper (Cu) sponges are reported. The scanning electron microscopy (SEM), transmission electron microscopy (TEM) images revealed the sponge-like and nanoparticles-like morphology of the metal sponges. The catalytic activity of the metal sponges was studied by the reduction of organic pollutants *viz.* 4-nitrophenol (4-NP), methyl orange (MO) and methylene blue (MB) in water. It was found that the Cu sponge was much faster for the reduction of 4-NP, MO, and MB, which was followed by the Co and Ni sponges, respectively. The metal sponges exhibited excellent catalytic stability for the reduction of 4-NP for multiple cycles. Additionally,

due to the magnetic properties, the Co and Ni sponges could be easily recovered and reused upon applying an external magnetic field.

1. Introduction

Catalyst plays a key role in chemical process industries by the transformation of raw materials into valuable products. A large portion of world economy is directly or indirectly associated with the performance of catalysts. It is considered that about 30% of the gross domestic product in European economies and the processing of over 80% of all manufactured products somehow is associated with catalysis.[1] Thus the development of catalyst is immensely important to make sure a global economic success and a sustainable society with fundamental aspects such as energy, food and water.

In this regard, transition and noble metal-based catalysts are some of the most widely used ones due to the availability, cheaper price, stability, and the extraordinary catalytic properties of these metals.[2,3,4,5] These catalysts are applied in a variety of chemical transformations[6] such as hydrogenations,[7] dehydrogenations,[8] alkylation,[9] amination,[10] and coupling reactions.[11] Recently, the application of catalysts for sustainable environmental remediation has garnered much attention.[12,13] For example, the catalytic degradation of organic pollutants,[14] catalytic reduction of nitrates[15] and hexavalent chromium,[16] catalytic dehydrohalogenation of halogenated compounds,[17] and advanced oxidation processes (e.g. fenton process)[18,19,20] are some of the important types of catalytic reactions that are of special interests. Catalytic processes for environmental remediation have advantages over other methods.[21] For example, the tunability in the reaction kinetics by tuning the morphology and the composition of the catalysts, the reusability, and cyclic stability. Therefore, the development of a self-supported and high-surface area (e.g. porous metals) catalyst based on facile method and

cheap and readily available metals is highly desirable. In terms of the metal, the transition metals are of prime choice due to their comparatively low price, availability, and intriguing catalytic properties. For example, porous Ni for the selective hydrogenation of carbonates into formic acid[22] and the use of Raney® Ni and Raney® Co for the hydrogenation of the organic compounds are some of the catalysts to mention. The porosity increases the surface area and opens the active sites of a metal, which are extremely important for the better performance of the catalysts. The porosity further facilitate elevated mass transport due to their higher surface areas.[23] Besides catalysis, porous metals have a great deal of applications including but not limited to electro/catalysis,[24] sorption,[25] fuel cell electrode materials,[26,] biofiltration,[27] hydrogen and energy storage,[28] supercapacitors and batteries[29,30], heat dissipation[31], and so on.

The commonly employed method for the preparation of self-supported porous metal include the templated synthesis, where solid template such as alumina, pumice, sugar crystal, NaCl crystal, polymer nanoparticles, etc. are used as the sacrificial materials.[32,33,34] Morphology-wise, the template can be porous or solid in nature and the morphology of the final porous metal is dependent on the morphology of the template. If the template is porous (such as porous alumina or pumice), the metal salt precursor is impregnated into the pores of the template. Thermal or chemical reduction of metal ion into the porous supports followed by the removal of the porous template make the porous metals. The porous metals prepared by this method usually have extraordinary higher specific surface area than the pure metal powders or foils.[35] The synthesis of the metal sponges or porous metals by the templated method has some drawbacks such as the requirement of multiple steps of synthesis and the necessity of the washing off the templates after the synthesis. In addition to the templated synthesis, there are template free synthesis methods where the porous metals could be synthesized by the direct chemical and

electrochemical reduction of the metal slats.[36,32] For example, Katla and colleagues reported the synthesis of porous gold, silver, platinum, and palladium nanosponges simply by the chemical reduction of the metal salts by sodium borohydride in aqueous solution.[37] However, these methods are limited to the synthesis of small amount of materials and may not be adapted to the large scale synthesis for the practical applications. Therefore, the development of a method for the synthesis of porous metals that does not require a template and can prepare a large amount of catalyst (porous metals) by a simple procedure with the adaptability for industrial scale production can be very lucrative in this area of research.

Herein, we report a facile method for the preparation of self-supporting and high-surface area transition metal (e.g. cobalt, nickel, and copper) sponges by heating a paste of metal salt and sucrose. The synthesis requires heating in two steps. In the first step, a mixture of metal nitrate salt and sucrose was heated at ~180 °C in the presence of air for about 30 min to obtain a foam-like substance. In the second step, foam-like substance was heated at 600 °C under argon to obtain the metal sponges. The utilization of sucrose as a soft sacrificial template for the preparation of metal sponges provides multiple advantages. For example, sucrose has reductive alcohol groups capable of reducing metal ions, which facilitates the nucleation and the growth of metallic clusters. Additionally, sucrose is a bio-derived organic compound having cheaper price, sucrose is readily available, and it is not associated with any kind of chemical hazards. To the best of our knowledge, the method presented here is novel and extremely simple in the sense of not requiring any harmful solvents and chemicals while at the same time avoiding multiple steps. Therefore, it could be readily extended to the fabrication of macroporous frameworks of various other transition metals, metal oxides, and their hybrid nanocomposites. Additionally, the method could be adapted for the industrial-scale production of the high-surface area metal, metal oxide

porous structures and their nanocomposites for numerous applications. The as-prepared metal sponges have been applied for the catalytic reduction of anthropogenic organic pollutants *viz.* 4-NP, MO, and MB in water. The reduction of 4-NP to 4-aminophenol (4-AP) is important with respect to the environmental remediation because of the toxic and carcinogenic nature of the 4-NP. Additionally, the 4-AP has usefulness as a photographic developer, corrosion inhibitor, precursor for the synthesis of paracetamol, etc.[38] On the other hand, the catalytic reduction of MO and MB can be considered as an intriguing method towards their reductive degradation for the purpose of water treatment.[39,40]

2. Materials and Methods

2.1. Materials

All the chemicals were used as received. Sucrose (>99.5%), $Co(NO_3)_2.6H_2O$ (99.999% trace metals basis), $Ni(NO_3)_2.6H_2O$ (99.999% trace metals basis), 4-nitrophenol ($O_2NC_6H_4OH \geq$ 99%), and sodium borohydride ($NaBH_4$ = 99%) were purchased from Sigma Aldrich. Methyl Orange ($C_{14}H_{15}N_3O_3S$ >98.0%) and methylene blue were obtained from TCI AMERICA and EMD Millipore Corporation, respectively. Milli-Q water (> 18.20 MI cm resistivity) was obtained from Milli-Q (Advantage A-10) water filter system.

2.2. Characterization Techniques

Agilent Cary 50 Conc UV-visible Spectrophotometer was used for the UV-visible studies. Quartz cuvette (10 mm path length) was used as the sample holder. Transmission electron microscopy (TEM) images were taken using a Hitachi H-7650 electron microscope. An acceleration voltage of 80 kV was used. Carbon filmed copper grids with 200 mesh (Electron microscopy sciences) were used for TEM imaging. A suspension of the metal sponge in ethanol was prepared by bath sonication and a drop of this suspension was deposited onto the grid and

air dried before imaging. Scanning Electron Microscopy (SEM) image and the Energy Dispersive X-ray (EDX) experiments were carried out using a Hitachi S-3400N Type II scanning electron microscope (SEM) equipped with an energy dispersive X-ray spectrometer. Carbon tape was used as the substrate for the SEM imaging. Bruker D8 Discover X-ray diffractometer with Cu Kα radiation (λ = 0.15418 nm) was used for the powder X-ray diffraction (XRPD) spectrum. Micromeritics ASAP 2020 Surface Area and Porosity Analyzer was used for nitrogen adsorption isotherms. Samples were weighed, heated at 150 ° C, and evacuated at 10 mmHg for 12 h before the adsorption measurements. After evacuation, nitrogen isotherms were obtained volumetrically at 77 K. The obtained data was fitted into the Brunauer-Emmett-Teller (BET) equation to determine the surface area.

2.3. Preparation of the Co, Ni, and Cu Sponges

All of the three metal sponges were prepared following the same experimental procedures. In detail, 400 mg sucrose and 4 mmol corresponding metal nitrate hydrate salt was mixed in a 100 ml glass beaker. The mixture was slowly melted on a hotplate heated at 120 °C. After heating and mixing on the hot plate for a while, a uniform viscous mixture was obtained. Then, the viscous mixture was immediately put in an oven, that was preheated to ~180 °C, for about 20 min. After this heating period a foam-like substance consisting of decomposed metal nitrate salts and sucrose was obtained. Since the decomposition of metal nitrate salts formed NO_2 and NOx gases, the furnace was placed in a fume hood with proper ventilation. Afterwards, the foam was annealed at 600 °C for 1 h in a tube furnace, under the flow of Argon, at a heating rate of 10 °C/min. For cooling, normal cooling rate of the furnace was utilized. After the furnace was completely cooled to room temperature the metal sponges were taken out from the furnace, which was stored under ambient condition for the characterization and catalytic applications.

For the synthesis of copper sponge, a minor modification was conducted. The mixture of sucrose and copper nitrate salt was first ground by a mortar and pestle and then the mixture was put into the oven at ~180 °C for the formation of foams.

2.4. Catalytic activity of the Co, Ni, and Cu Sponges

The catalytic performance of metal sponges was evaluated by the reduction of 4-nitrophenol (4-NP), methyl orange (MO), and methylene blue (MB) in water, Scheme 1. Excess sodium borohydride ($NaBH_4$) was used as the reducing agent. As $NaBH_4$ spontaneously decomposes in water, it is usually used in excess. The reduction of 4-NP, MB, and MO was monitored by the gradual decrease of their characteristic absorbance at 400, 464, and 665 nm, respectively with aid of UV-visible spectrophotometer.[41,42,43]

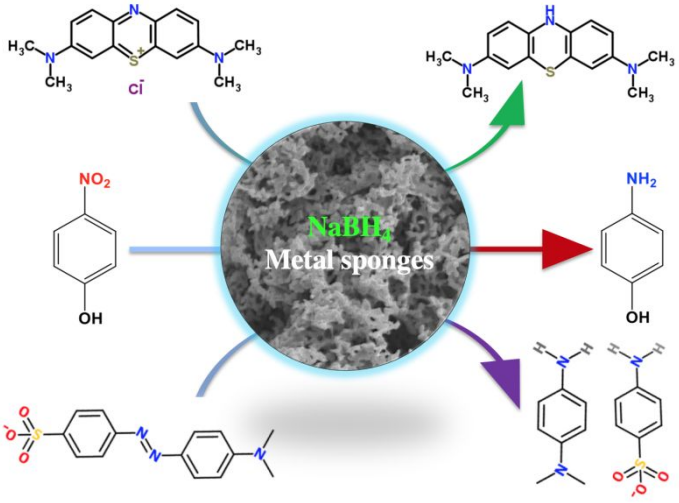

Scheme 1. Scheme for the metal sponges catalyzed reduction of 4-NP, MO, and MB in water by the $NaBH_4$.

For the reduction of 4-NP, 10 mL of 4-NP aqueous solution (0.2 mM) was mixed with 10 mg of the metal sponges by 10 min of bath sonication in a glass scintillation vial. Afterwards, 1 mL of freshly prepared $NaBH_4$ aqueous solution (50 mg $NaBH_4$ in 1mL water) was added into

the reaction mixture and the reaction course was monitored by using the UV-visible spectrophotometer.

For the catalytic reduction of MB and MO, same experimental procedure was followed except the concentration of MB and MO solution used was 15 ppm and 25 mg $NaBH_4$ in 1 mL water used as the reducing agent. The time dependent decolorization/reduction of MB and MO was monitored by their characteristic absorbance at 665 and 464 nm, respectively.

3. Results and Discussion

3.1. Synthesis of the Metal Sponges

The synthesis of Co, Ni, and Cu metal sponges was carried out by heating a paste consisting of metal nitrate salt and sucrose (commonly known as table sugar), Scheme 2. The heating was performed in three steps. First, a mixture of the sucrose and metal nitrate salt was slowly melted on a hot plate at 120 °C to obtain a uniform viscous paste. Then, the paste was immediately heated at ~180 °C in a box furnace in the presence of air to obtain a foam-like composite. The foam-like composite consisted of partially carbonized sucrose and partially decomposed metal salts, Equation 1. When heated at this temperature, the nitrate salts started to decompose to generate different gases (Equation 1), which caused the sticky mixture to blow up in the form of foam-like composite during the heating process.[44] The generation of the gases induced the porosity of the foam-like composite and eventually in the metal sponges.

$$C_{12}H_{22}O_{11}\,(s) + Co(NO_3)_2.6H_2O(s) \rightarrow C_{foam} + CoO\,(s) + N_2(g) + H_2O\,(g) + NO_x\,(g) \qquad (1)$$

$$C_{foam} + CoO\,(s) \rightarrow Co\,(s) + CO_2(g) \qquad (2)$$

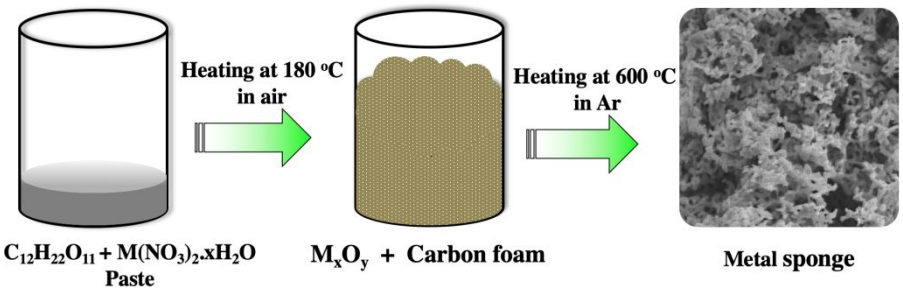

Scheme 2. Scheme showing different stages for the preparation of metal sponges. a) mixture of metal nitrate salt and sucrose; b) metal nitrate decomposition into a foam-like composite; c) further heating of the foam in argon to obtain the metal sponges.

Finally, the foam-like composite was further heated at 600 °C in presence of argon to obtain the porous metal with the presence of a trace amount of carbon, Equation 2. When heated at 600 °C in argon atmosphere, the partially decomposed metal salt (metal oxide mostly) undergone carbothermal reduction forming porous metallic frameworks. In the carbothermal reduction, the carbon gets oxidized to form CO_2 gas while reducing metal oxides to zero valent metals. The generation of CO_2 gas may have caused additional porosity of the metallic sponges. Incomplete oxidation may have left behind trace of carbon in the porous metal catalysts.

The advantage of the method is that the experimental conditions is simple, fast, and adaptable to industrial scale. Moreover, the method does not require any expensive or hazardous reagents, experimental conditions, and post-synthesis modifications or treatments. The method could be adapted for the industrial-scale production of the high-surface area metal, metal oxide porous structures and their nanocomposites for numerous applications. We also assume that the method can be employed to prepare metals of different pore size and surface area by varying the experimental conditions and parameters such as metal precursor to the sucrose molar ratio, heating temperature and rate, etc.

3.2. Characterization of the Metal Sponges

The metal sponges were thoroughly characterized in terms of the morphology, crystallinity, specific surface area, and the thermal stability analyses. The. SEM and TEM images were taken to study the nanoscale morphology of the metal sponges. The elemental compositions of the metal sponges were qualitatively and quantitatively determined by the SEM-EDS analysis. The crystallinity and specific surface area and thermal stability of the metal sponges were investigated by the XRPD, BET surface area analysis, and the thermal gravimetric analysis.

3.2.1. SEM Images of the Metal Sponges

The SEM image analysis revealed the porous morphology of the as-synthesized cobalt, nickel, and copper sponges, Figure 1. For instance, the SEM image of the Co sponge (Fig. 1a,1b) demonstrated a self-supported three-dimensional interconnected network consisting of thin filaments. The filaments were seen to be nanoassembled and entangled together to form a 3 dimensional-interconnected structure. Further magnification revealed that the filaments were not uniform in terms of size and shape, figure 1b. The filaments were often seen to have many branches indicating their formation during the foam formation and/or carbothermal reduction step of synthesis. A porous morphology with a high volume of void space was also observed from the SEM images. This void space and the porous structure induced the high specific surface area of the metal sponges, which is very important for the purpose of catalysis.

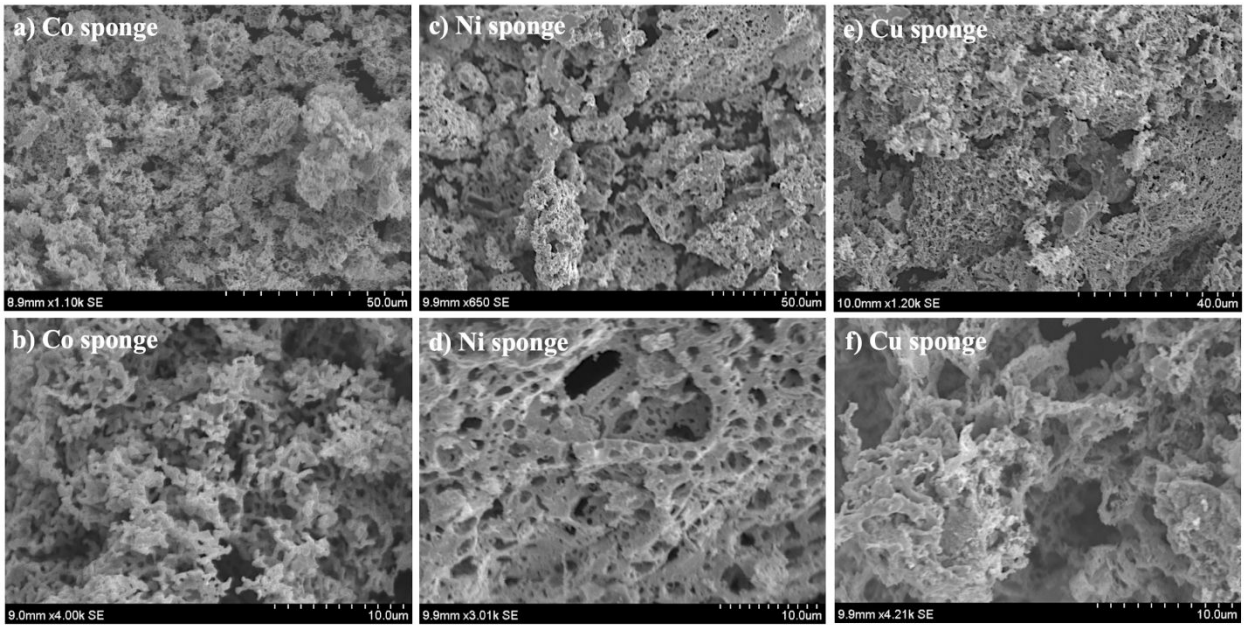

Figure 1. Typical SEM images of the cobalt, nickel, and copper sponges with different magnifications showing the morphology.

Similarly, the SEM images of the Ni and Cu sponges revealed the porous morphology, Figure 1c-1f. The porosity and void spaces of the Ni and Cu sponges can be clearly seen in the SEM images. However, the Ni and Cu sponges were found to be less porous and filamentous as compared to the Co sponge. This indicate the less surface area of the Ni and Cu sponges compared to the Co sponge, which is further supported by the BET surface area analysis. Morphology-wise, the Ni and Cu sponges were seen to be more like two-dimensional sheet like structure with perforations.

3.2.2. EDX Spectrum of the Metal Sponges

The EDX spectrum was carried out to determine the qualitative and quantitative elemental analysis of the metal sponges, Figure 2. For example, Figure 1a demonstrates EDX peaks that are corresponding to cobalt, oxygen, and carbon. A high intensity of the cobalt peak indicates that the sponge is consisting of mostly cobalt metal, whereas; less intense peaks of

carbon and oxygen indicates that there is some amount of carbon and oxygen in the cobalt sponge. Oxygen peak may have arisen from the protective oxide layer on the metal sponges. Likewise, the EDS spectrum of the nickel, and copper sponges showed a high abundance of nickel and copper with comparatively low abundance of carbon and oxygen. The strong cobalt, nickel, and copper peaks indicate that the sponges are mostly metallic in nature. However, the carbon and oxygen peaks indicate that the sponges have some percentage of carbon too. The crystalline metallic nature of the metal sponges was further analyzed by the XRPD analysis (discussed below).

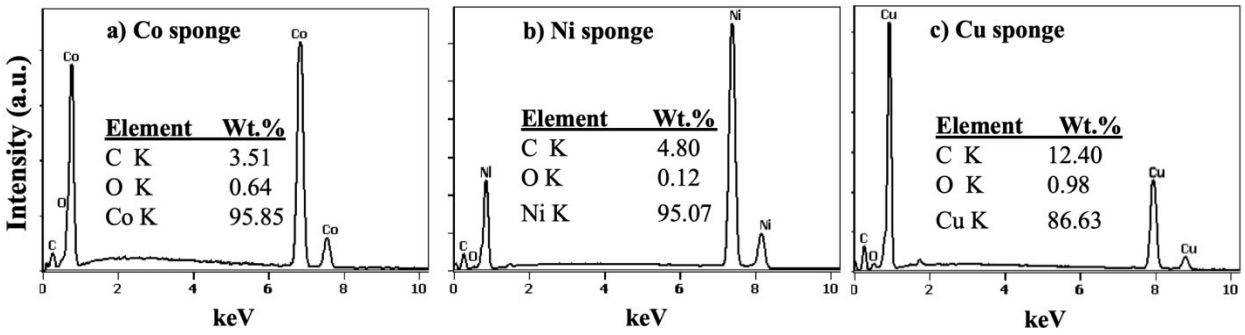

Figure 2. EDX spectrum of the a) cobalt, b) nickel, and c) copper sponges showing the qualitative and quantitative elemental composition.

The percent elemental composition of the metal sponges, obtained from the EDS analysis, is also shown in Figure 2. It was found that the Co sponge had about 3.5 % C, 0.6 % oxygen, and 95.8 % metallic cobalt. The Ni sponge was composed of about 4.8 % C, 0.1 % oxygen, and 95.1 % metallic nickel, whereas; the Cu sponge was composed of about 12.4 % C, 1.0 % oxygen, and 86.6 % metallic copper.

3.2.3. TEM Images of the Metal Sponges

The TEM image analysis was further performed to characterize the morphology of the metal sponges. Typical TEM images of the metal sponges with different magnifications are shown in Figure 3. From the TEM images it was found that the metal sponges had two different

morphologies. For example, the Co sponge was seen have two different morphologies viz. the sponge-like and the particle-like morphologies that are shown in Figure 3a and 3b, respectively. Further analysis revealed that the sponge like morphology (Figure 3a) consisted of filamentous metal nanowire of varying dimensions and it was mostly observed where there was no carbon film associated. We assume that the sponge-like morphology may have formed due to the fusion and aggregation of the smaller nanoparticles during the high-temperature heating steps of the synthesis. However, the particles like morphology was observed where there was carbon film, Figure 3b. The carbon film was originated from carbonization of sucrose and the metallic nanoparticles were seen to have varying particle sizes. We assume that the carbon film may have coated the metallic nanoparticles and prevented their further growth and aggregation leading to the sponge like morphology.

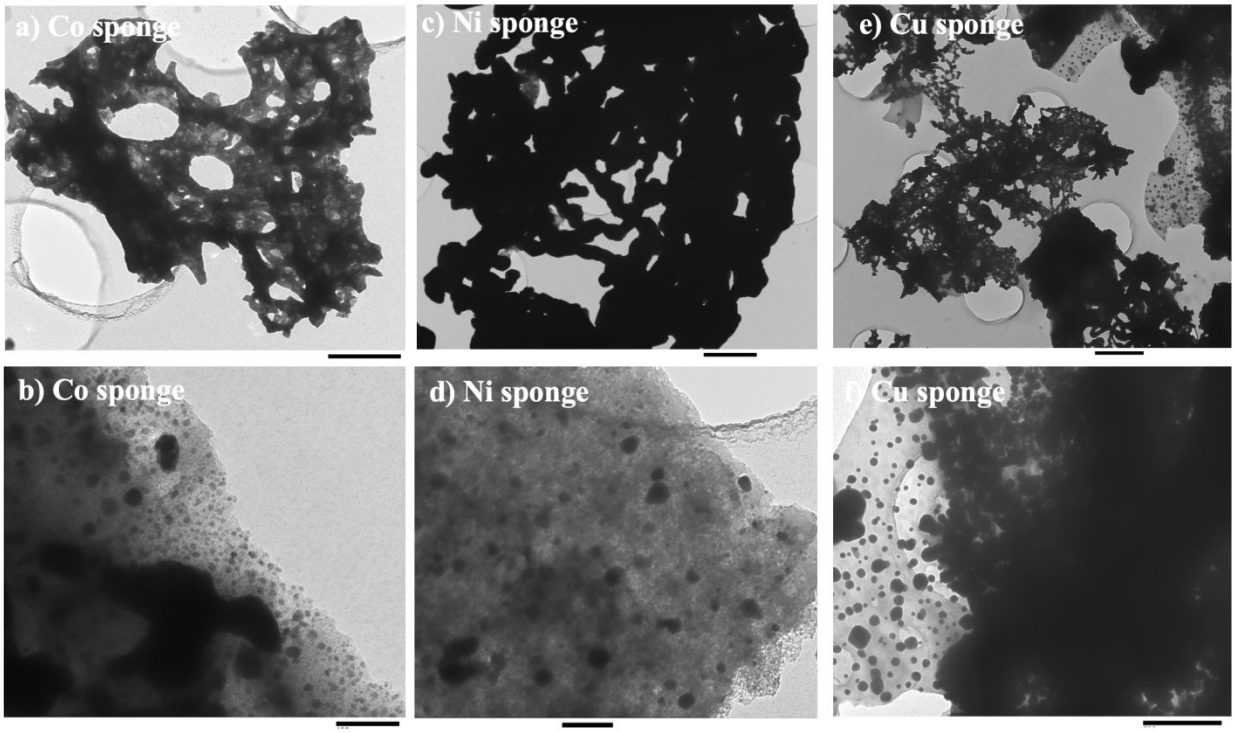

Figure 3. TEM images of cobalt, nickel, and copper sponges showing the sponge-like and nanoparticles-like morphologies. Scale bars: 500, 100, 1000, 100, 1000, and 500 nm for figures a through f, respectively.

Like the Co sponge, the Ni and Cu sponges demonstrated two types of morphologies. The average thickness of the Co, Ni, and Cu filaments in the sponges were calculated to be 56, 230, and 120 nm, respectively. The average size of the Co, Ni, and Cu nanoparticles in the sponges were calculated to be 9.5, 21, and 41 nm, respectively.

3.2.4. XRPD Pattern of the Metal Sponges

The X-Ray powder diffraction patterns were obtained to determine the crystalline properties of the metal sponges. The XRPD pattern of the Co sponge is shown in Figure 4a. The diffraction peaks located at $2\theta = 44.1^{\circ}$, 51.5° and 75.8° can be attributed to the 111, 200, and 220 crystalline faces of the metallic cobalt.[45] Moreover, this type of diffraction peaks corresponds to the face-centered-cube (fcc) crystalline phase of the metallic cobalt.[46] The absence of any other undesired peaks indicate that the cobalt sponge is highly pure with crystalline metallic property and it has low or undetectable amount of cobalt oxides on it. This result is compatible with the EDS studies that were discussed above.

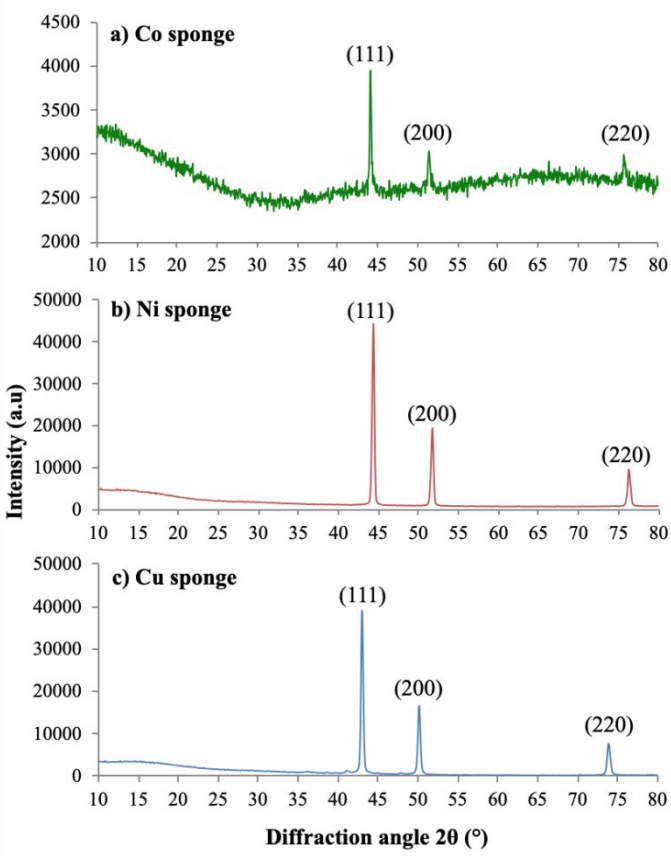

Figure 4. XRPD pattern of the a) cobalt, b) nickel, and c) copper sponges showing the crystalline structure.

Similarly, the XRD pattern of the Ni and Cu sponges are shown in Figure 4b and 4c. The XRPD patterns of the Ni (2θ = 44.3°, 51.7° and 76.1°) and Cu (2θ = 43.9°, 50.1° and 73.8°) sponges correspond to the face-centered cube (fcc) phase of the crystal lattice.[47],[48] Additionally, the highly intense peaks of the Ni and Cu sponges without having additional peaks indicate their high purity, crystallinity, and the presence of no or undetectable amount of oxide layer on them. The Debye-Scherrer's Formula (Equation 3) was employed to determine the average crystallite size of the metal sponges. The XRPD peak corresponding to the (111) crystalline face was utilized in this regard.[49]

$$d = k\lambda / \beta \, Cos(\theta) \qquad (3)$$

where d is the crystallite size, k is the shape factor (0.9), λ is the wavelength of Cu Kα X-ray radiation (1.54 Å), θ is the Bragg diffraction angle, and β is the full width at half maximum of the respective diffraction peak. Employing the Debye-Scherrer formula, the average crystallite size of the Co, Ni, and Cu sponges where calculated to be 38.9, 25.6, and 27.3 nm, respectively. It could be observed that the crystallite sizes of the metal sponges, obtained from the XRPD analysis, were different from the average particle size measured by the TEM analysis. This because of the fact that the crystallite size is the size of a coherently diffracting domain of a crystal in a particle and it is not necessarily be same as the particle size determined from the TEM images.

3.2.5. Surface Area analysis of the Metal Sponges

The specific surface area, pore size, and pore volume of the metal sponges were measured using nitrogen gas adsorption analysis. Table 1 shows the BET surface area, pore size, and pore volume of the metal sponges obtained from the N_2 adsorption experiments. As can be seen from the BET analysis that the cobalt sponge had the greatest surface area ca. 17.3935 m^2/g, while copper has the least surface area of the three at 2.7280 m^2/g. The Ni sponge had the BET surface area of about 8.85 m2/g.

Table 1. BET surface area, total pore volume, and average pore diameter of the Co, Ni, and Cu sponges.

Sample	BET surface area (m2/g)	Total pore volume (cm3/g)	Average pore diameter (nm)
Co Sponge	17.3935 m^2/g	0.006750 cm^3/g	67.731 Å
Ni Sponge	8.8472 m^2/g	0.003236 cm^3/g	74.118 Å
Cu Sponge	2.7280 m^2/g	0.004188 cm^3/g	66.102 Å

This difference in surface can be correlated to the porosity and void spaces of the metal sponges, shown in the SEM images, Figure 1. correlates to the pore volume and pore diameter. Observing the SEM image, the difference in porosity is observable. The SEM images revealed that the Co sponge had much higher porosity and void space compared to the Ni and Cu sponges and thereby the Co sponge demonstrated the highest BET surface area. The comparative pore volume and average pore diameter of the metal sponges are also given in Table 1.

3.2.6. Thermogravimetric Analysis

In order to further quantify the percent amount of carbon in the metal sponges the thermal gravimetric analysis was carried out. As shown in Figure 5, the metal sponges lost less than 5 % weight what heated to about 800 °C.

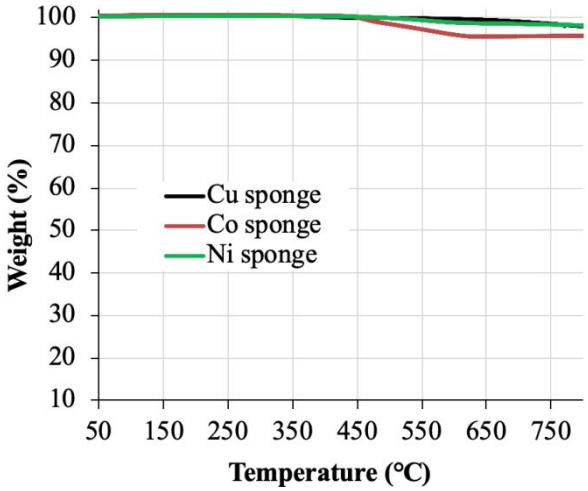

Figure 5. Thermal decomposition profile of the metal sponges showing the percent carbon in the sponges.

This indicate that percent weight of carbon in the metal sponges. From the results of this study it was found that the Co, Ni, and Cu sponges had only about 4.2, 1.7, and 1.8 weight percent carbon in the sponges.

3.3. Catalytic Activity of the Co, Ni, and Cu Sponges

The catalytic activity of the Co, Ni, and Cu sponges was studied by their ability to reduce 4-NP, MO, and MB in water with $NaBH_4$ at the unadjusted pH. The reduction of 4-NP, MO, and MB with NaBH4 was monitored by the UV-visible spectroscopy by the lowering of their characteristic absorption bands at 400, 464, and 665 nm, respectively. The reaction could be observed by the naked-eye too by the decolorization of the inherent color of the substrates. The experimental results of the catalytic reactions were analyzed by the pseudo-first-order rate equation, which is expressed as follows:

$$-\ln(C_t/C_0) = kt. \qquad (4)$$

where C_0 and C_t represent the initial and time-dependent concentrations of the substrates, respectively. The time-dependent percent reduction of 4-NP, MO, and MB was calculated by using the following equation:

$$Percent\ reduction = \frac{Co - Ct}{Co} \times 100\% = \frac{Ao - At}{Ao} \times 100\% \qquad (5)$$

where A_o and A_t represent the the initial and time-dependent absorbance of 4-NP, MO and MB at 400, 464, and 665 nm, respectively.

To study the mechanism of the reaction, the Langmuir−Hinshelwood model was utilized. Langmuir−Hinshelwood model suggests that the reaction proceeds through the concomitant adsorption of the reducing agent and the substrate on the catalyst surfaces to complete the reaction.[50,51]

3.3.1. Catalytic Reduction of 4-NP

The catalytic reduction of 4-NP by the metal sponges is shown in Figure 6. The reaction was studied up to 10 min period of time and within which the reaction proceeded to more than completion. The reaction was monitored by the time-dependent UV-visible absorption spectrum

of 4-nitrophenolate. A representative UV-visible absorption spectrum of 4-nitrophenolate is shown in Figure 6a. A gradual decrease in the absorbance at 400 nm is characteristic to the reduction of 4-NP; whereas the increase in the absorbance at 300 nm is characteristic to the formation of 4-AP, which could be clearly observed from Figure 6a.

The time-dependent percent reduction of 4-NP by the metal sponges is shown in figure 6b. It was found that the Cu sponge was the most active in doing the reduction, which was followed by the Co, and Ni sponges, respectively. Cu sponge took about 1 min to completely reduce the 4-NP into 4-AP, whereas Co and Ni sponges took about 6 min and 10 min to reduce more than 95 % of the 4-NP, respectively. In contrast, the reduction of 4-NP in the absence of catalyst showed negligible amount of reduction, which indicated the robustness of 4-NP to undergo reduction without the catalyst.

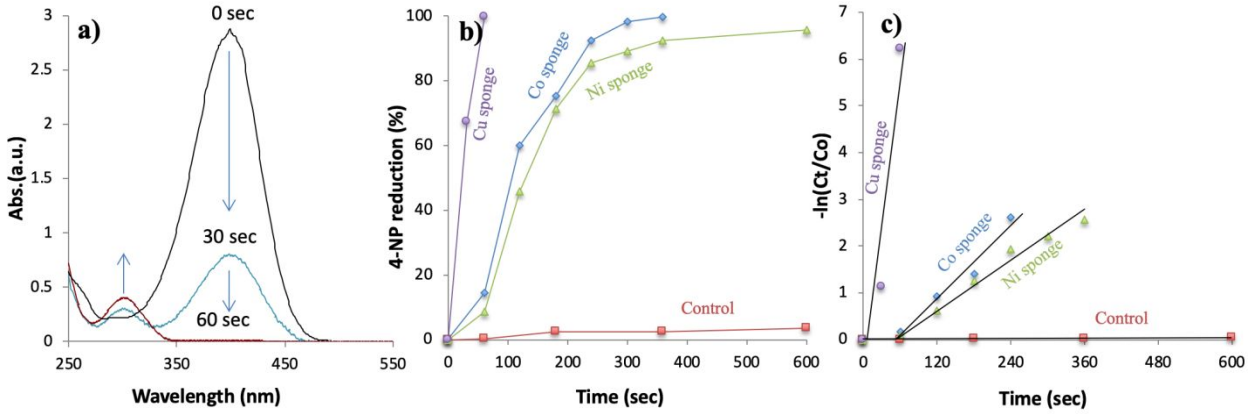

Figure 6. Time-dependent a) UV-visible spectrum of 4-NP during its reduction on the Cu sponge, b) percent reduction of 4-NP catalyzed by different metal sponges, and c) Pseudo-first order reaction kinetics of the catalytic reduction of 4-NP.

The kinetics of the catalytic reduction of 4-NP by the Co, Ni, and Cu sponges is shown in Figure 6c. The experimental results followed a linear relationship when $-\ln(C_t/C_0)$ was plotted against reaction time (t) (Equation 4). This suggested that the reduction followed the pseudo-first

order kinetics, which makes sense as $NaBH_4$ was used in a large excess in the reaction. The apparent rate constant (k_{app}) of the reduction of 4-NP was obtained directly from the slope of the straight line of the $-\ln(C_t/C_0)$ vs. time (t) graph. For the Co, Ni, and Cu sponge the k_{app} was calculated to be 1.31×10^{-2} s^{-1}, 9.10×10^{-3} s^{-1} and 1.04×10^{-1} s^{-1}, respectively. The k_{app} of the uncatalyzed reaction was calculated to be 6.0×10^{-5} s^{-1}, which is much slower than the Co, Ni, and Cu sponges catalyzed reactions.

The linear behavior of the $-\ln(C_t/C_0)$ vs. time (t) graph indicated that all the reaction followed the Langmuir–Hinshelwood (LH) model. This further suggested that the reduction of 4-NP happened through the simultaneous adsorption of the sodium borohydride and the 4-nitrophenolate on the surface of the metal sponges.

3.3.2. Catalytic Reduction of Methyl Orange (MO)

The reduction of MO with $NaBH_4$ using the metal sponges as catalysts is shown in Figure 7. The gradual decrease in absorbance at 464 nm and 275 nm corresponds to the reduction of MO and the gradual increase in absorbance at 245 nm corresponds to the formation of 4-aminobenzenesulfonate and 4-N,N-dimenthylaminobenzene, Figure 7a. The time-dependent percent reduction of MO to 4-aminobenzenesulfonate and 4-N,N-dimenthylaminobenzene by the metal sponges is shown in figure 7b. The Cu sponge showed higher activity for the reduction of MO than the Co and Ni sponges. In the absence of catalyst, a minor reduction of MO was observed, however it is insignificant in comparison to the metal sponges catalyzed ones.

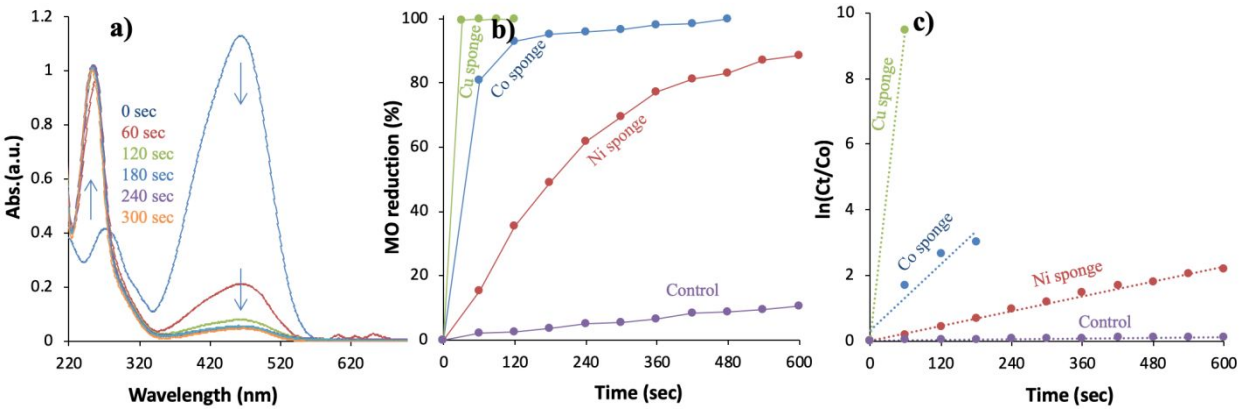

Figure 7. Time-dependent a) UV-visible spectrum of MO during its reduction on the Co sponge, b) percent reduction of MO catalyzed by different metal sponges, and c) Pseudo-first order reaction kinetics of the catalytic reduction of MO.

The kinetics of MO reduction by the metal sponges is shown in Figure 7c demonstrating a linear relationship following the LH model, which also suggests a pseudo-first order kinetics as $NaBH_4$ was used in excess. The k_{app} for the Co, Ni, and Cu sponge was calculated to be 1.67 $\times 10^{-2}$ s^{-1}, 3.8 $\times 10^{-3}$ s^{-1} and 1.58 $\times 10^{-1}$ s^{-1}, respectively. The k_{app} of the uncatalyzed reaction was calculated to be 2.0 $\times 10^{-4}$ s^{-1}, which is many times slower than the metal sponge catalyzed reactions.

3.3.3. Catalytic Reduction of MB

The catalytic reduction of MB on the metal sponges is shown in Figure 8. Like 4-NP and MO, the reaction of MB was monitored by its reductive decolorization. During the catalysis, a gradual decrease in the characteristic absorbance of MB at 300 and 665 nm was observed, Figure 8a.[52] The deep blue colored MB turned into a colorless reduced product viz. leucomethylene blue. The time-dependent percent reduction of MB by different metal sponges is shown in figure 8b. Out of the three sponges, it was found that the Cu sponge had the most catalytic activity, which was followed by the Co, and Ni sponges, respectively. The Cu sponge took about 1 min to

completely reduce the MB, whereas Co and Ni sponges took about 6 min and 10 min to reduce more than 95 % of the MB, respectively. When doing a control experiment without the catalyst, about 10 % reduction of MB was observed, which indicated that the metals sponges were responsible for its catalytic reduction.

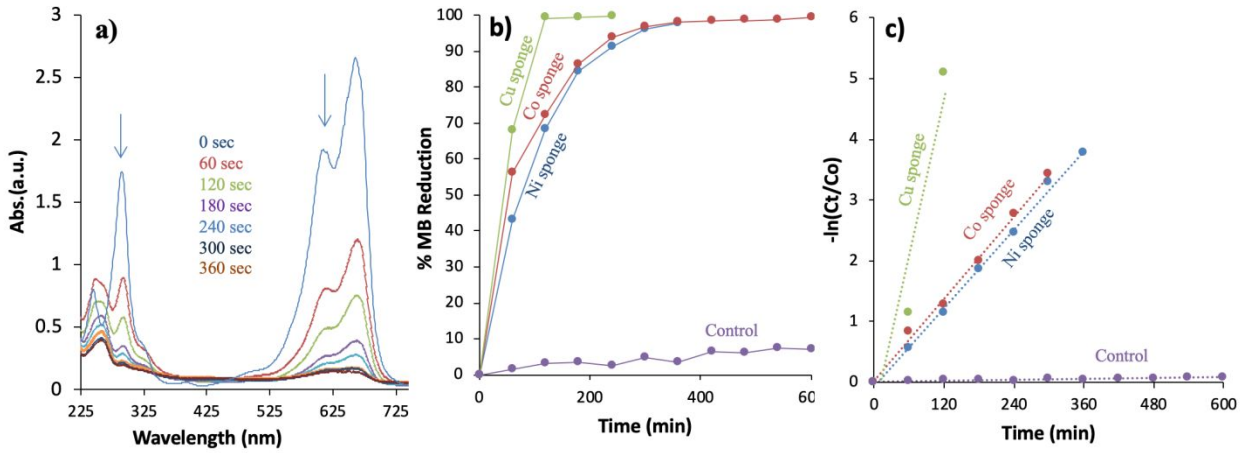

Figure 8. Time-dependent a) UV-visible spectrum of MB during its reduction on the Ni sponge, b) percent reduction of MB catalyzed by different metal sponges, and c) Pseudo-first order reaction kinetics of the catalytic reduction of MB.

The kinetics of the catalytic reduction of MB is shown in Figure 8c. The experimental results followed a linear relationship when $-\ln(C_t/C_0)$ was plotted against reaction time (t) (Equation 4). This suggested that the reduction followed the pseudo-first order kinetics and Langmuir–Hinshelwood (LH) model. For the Co, Ni, and Cu sponges the k_{app} was calculated to be 1.13 $\times 10^{-2}$ s^{-1}, 1.08 $\times 10^{-2}$ s^{-1}, and 4.24 $\times 10^{-2}$ s^{-1}, respectively. The k_{app} of the uncatalyzed reaction was calculated to be 1.0 $\times 10^{-4}$ s^{-1}, which indicates the robustness of MB to undergo reduction without the catalysts.

To avoid any confusion that the 4-NP, MO, and MB may have adsorbed on the metal sponges during the catalysis, several control experiments were carried out. For this, mixture of

substrates (4-NP, MO, and MB solutions) and metal sponges were bath sonicated for 10 min. Afterwards, the percent adsorption was calculated. For all three metal sponges, less than 5 percent adsorption was obtained. This eventually confirms that the decolorization of the 4-NP, MO, and MB solutions happened due to the catalytic reduction, not by physical adsorption.

The catalytic performance of the metal sponges for the reduction of 4-NP, MO, and MB is compared with other transition metal catalysts in Table 2. All of the catalytic processes summarized in the table below employed $NaBH_4$ as the reduction agent. By comparison, the Co, Ni, and Cu sponges demonstrated higher/similar catalytic activities compared to various other transition metal catalyst systems reported in the literature.

Table 2. Comparisons of catalytic performance of the Co, Ni, and Cu sponges for reduction of 4-NP, MO, and MB Over various transition metal catalyst systems

Catalysts	Substrate	Rate constant (s^{-1})	References
Co sponge	4-NP	1.31×10^{-2}	This work
Co sponge	MO	1.67×10^{-2}	This work
Co sponge	MB	1.13×10^{-2}	This work
Ni sponge	4-NP	9.10×10^{-3}	This work
Ni sponge	MO	3.8×10^{-3}	This work
Ni sponge	MB	1.08×10^{-2}	This work
Cu sponge	4-NP	1.04×10^{-1}	This work
Cu sponge	MO	1.58×10^{-1}	This work
Cu sponge	MB	4.24×10^{-2}	This work
p(MAc)–Cu	4-NP	$\sim 2.7 \times 10^{-2}$	[53]
p(MAc)–Co	4-NP	$\sim 1.4 \times 10^{-2}$	[53]
p(MAc)–Ni	4-NP	$\sim 1.25 \times 10^{-2}$	[53]
p(MAc)–Cu	MO	$\sim 2.5 \times 10^{-2}$	[53]
p(MAc)–Co	MO	$\sim 4 \times 10^{-3}$	[53]
p(MAc)–Ni	MO	$\sim 2 \times 10^{-3}$	[53]
p(TA)-Cu	MB	$\sim 1.13 \times^{-2}$	[54]

Cu microsphere	MB	~6.55 $\times^{-3}$	[55]
Ni nanotube arrays	MB	~3.7 $\times^{-2}$	[56]
Ni/CPM-1	MB	~9.71 $\times^{-3}$	[57]
Ni/CPM-2	MB	~9.51 $\times^{-3}$	[57]
p(TA)-Co	4-NP	~7.16 $\times^{-3}$	[54]
Amid-p(MAc-co-AN)–Cu	4-NP	~7.08 $\times^{-3}$	[58]
Amid-p(MAc-co-AN)–Co	4-NP	~1.24 $\times^{-3}$	[58]

Moreover, the Co, Ni, and Cu sponges have the advantages of easy separation (centrifugation or magnetic decantation) and being highly stable allowing recycling and reusability. Most importantly, the facility of the synthesis methodology of the catalysts could be employed or adapted for the large-scale production in the industrial setup.

3.3.4. Stability of the Metal Sponges for the Reduction of 4-nitrophenol

Cyclic stability and reusability are two important and desired properties of the catalysts. The cyclic stability of the metal sponges was demonstrated by the catalytic reduction of 4-NP for five cycles. For the cyclic stability of the Co, Ni, and Cu sponges, the percent reduction of 4-NP was calculated after 6, 10, and 1 min of reaction, respectively. The percent reduction of 4-NP to 4-AP was calculated by the use of UV-visible spectroscopy and Equation 5. For example, when Cu sponge was used, percent reduction of 4-NP was calculated after 1 min of reaction in each cycle of catalysis. Afterwards, the catalyst was separated from reaction mixture by centrifugation, washed with deionized water and reused in the same manner. For the Co and Ni sponges, percent reduction of 4-NP was calculated after 6 and 10 min of reaction, respectively in every cycle. The catalysts were separated by magnetic decantation, washed with deionized water and was reused for the following cycles.

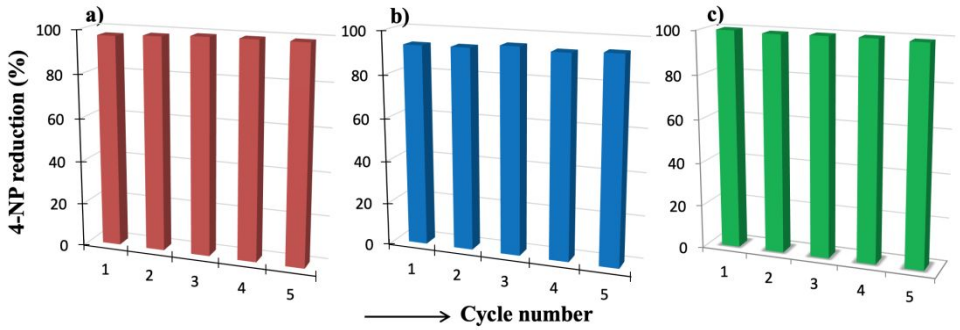

Figure 9. Cyclic stability of the a) Cobalt b) Nickel, and c) Copper sponges for the reduction of 4-NP.

Figure 9 demonstrates the cyclic stability of the metal sponges for the 4-NP reduction. It was found that all of the three metal sponges were highly stable for the reduction of 4-NP throughout the cycles. It showed that the Co and Cu sponged could effectively reduce more than 98 % of the 4-NP in every cycle of the reaction. Whereas, the Ni sponge reduced up to 96 % 4-NP in every cycle. No or negligible drop of catalytic activity was observed throughout the cycles, which indicated the robustness of the catalysts. Therefore, from this study it could be concluded that the Co, Ni, and Cu sponges could potentially be used a highly stable and efficient catalyst for the reduction of 4-NP in water.

4. Conclusions and Summary

A simple method for the preparation of porous cobalt, nickel, and copper sponges by heating a mixture of sucrose and metal nitrate salts is reported. The metal sponges were found to have high porosity with particles and filamentous morphology. All of the three metal sponges demonstrated excellent catalytic activity for the reduction of 4-nitrophenol, methyl orange, and methylene blue in water in the presence of $NaBH_4$. Excellent cyclic stability of the sponges indicated their robustness and potential application in a variety of other catalytic reactions. Also,

from the synthesis methodology perspective, the procedure could be adapted for the preparation of a wide variety of transition and mixed metal sponges for numerous applications.

Author Information

Corresponding Authors:

Md Tariqul Islam, Email: mtislam@miners.utep.edu / tariqul.lab@gmail.com

Juan C. Noveron, Email: jcnoveron@utep.edu

Notes

The authors declare no conflicting financial interest.

Acknowledgement

Financial support from NSF grants CHE-0748913, the NEWT-1449500, and USDA 2014-38422-22078 are gratefully acknowledged. Authors would like to thank Dr. Huiyao Wang for the kind assistance with TEM and SEM imaging techniques.

References

[1] Catlow, C. Richard, et al. "Catalysis making the world a better place." (2016): 20150089.

[2] Zassinovich, G., Mestroni, G., & Gladiali, S. (1992). Asymmetric hydrogen transfer reactions promoted by homogeneous transition metal catalysts. *Chemical Reviews*, *92*(5), 1051-1069.

[3] Cokoja, M., Bruckmeier, C., Rieger, B., Herrmann, W. A., & Kuehn, F. E. (2011). Transformation of carbon dioxide with homogeneous transition-metal catalysts: a molecular solution to a global challenge?. *Angewandte Chemie International Edition*, *50*(37), 8510-8537.

[4] Ishijima, M., Huaman, J. L. C., Yokoyama, S., Shinoda, K., Uchikoshi, M., Miyamura, H., & Jeyadevan, B. (2018). In situ spectroscopic studies of the one-pot synthesis of composition-controlled Cu–Ni nanowires with enhanced catalytic activity. *New Journal of Chemistry*, *42*(15), 13044-13053.

[5] Sahiner, N., & Butun, S. (2015). The Use of Cu, Ni and Co Metal Nanoparticles Generated in Acidic Hydrogels as Catalysts in the Reduction of Nitro Phenols. *Journal of Hydrogels*, *1*(1), 63-69.

[6] Kallmeier, F., & Kempe, R. (2018). Manganese complexes for (De) hydrogenation catalysis: a comparison to cobalt and iron catalysts. *Angewandte Chemie International Edition*, *57*(1), 46-60.

[7] Tomishige, K., Nakagawa, Y., & Tamura, M. (2017). Selective hydrogenolysis and hydrogenation using metal catalysts directly modified with metal oxide species. *Green Chemistry*, *19*(13), 2876-2924.

[8] Zhan, W. W., Zhu, Q. L., & Xu, Q. (2016). Dehydrogenation of ammonia borane by metal nanoparticle catalysts. *Acs Catalysis*, *6*(10), 6892-6905.

[9] Huang, F., Liu, Z., & Yu, Z. (2016). C-Alkylation of Ketones and Related Compounds by Alcohols: Transition-Metal-Catalyzed Dehydrogenation. *Angewandte Chemie International Edition*, *55*(3), 862-875.

[10] Park, Y., Kim, Y., & Chang, S. (2017). Transition metal-catalyzed C–H amination: Scope, mechanism, and applications. *Chemical reviews*, *117*(13), 9247-9301.

[11] Choi, J., & Fu, G. C. (2017). Transition metal–catalyzed alkyl-alkyl bond formation: another dimension in cross-coupling chemistry. *Science*, *356*(6334), eaaf7230.

[12] Fujiwara, K., Okuyama, K., & Pratsinis, S. E. (2017). Metal–support interactions in catalysts for environmental remediation. Environmental Science: Nano, 4(11), 2076-2092.

[13] Liu, X., Iocozzia, J., Wang, Y., Cui, X., Chen, Y., Zhao, S., ... & Lin, Z. (2017). Noble metal–metal oxide nanohybrids with tailored nanostructures for efficient solar energy conversion, photocatalysis and environmental remediation. *Energy & Environmental Science*, *10*(2), 402-434.

[14] Zeng, T., Zhang, X., Wang, S., Niu, H., & Cai, Y. (2015). Spatial confinement of a Co3O4 catalyst in hollow metal–organic frameworks as a nanoreactor for improved degradation of organic pollutants. *Environmental science & technology*, *49*(4), 2350-2357.

[15] Sá, J., & Vinek, H. (2005). Catalytic hydrogenation of nitrates in water over a bimetallic catalyst. *Applied Catalysis B: Environmental*, *57*(4), 247-256.

[16] Omole, M. A., K'Owino, I. O., & Sadik, O. A. (2007). Palladium nanoparticles for catalytic reduction of Cr (VI) using formic acid. *Applied Catalysis B: Environmental*, *76*(1-2), 158-167.

[17] Tavoularis, G., & Keane, M. A. (1999). Gas phase catalytic dehydrochlorination and hydrodechlorination of aliphatic and aromatic systems. Journal of Molecular Catalysis A: Chemical, 142(2), 187-199.

[18] Andreozzi, R., Caprio, V., Insola, A., & Marotta, R. (1999). Advanced oxidation processes (AOP) for water purification and recovery. *Catalysis today*, *53*(1), 51-59.

[19] Islam, M. T., Jing, H., Yang, T., Zubia, E., Goos, A. G., Bernal, R. A., ... & Noveron, J. C. (2018). Fullerene stabilized gold nanoparticles supported on titanium dioxide for enhanced photocatalytic degradation of methyl orange and catalytic reduction of 4-nitrophenol. *Journal of environmental chemical engineering*, *6*(4), 3827-3836.

[20] Islam, M. T., Dominguez, A., Alvarado-Tenorio, B., Bernal, R. A., Montes, M. O., & Noveron, J. C. (2019). Sucrose-Mediated Fast Synthesis of Zinc Oxide Nanoparticles for the Photocatalytic Degradation of Organic Pollutants in Water. *ACS Omega*, *4*(4), 6560-6572.

[21] Sahiner, N., & Butun, S. (2015). The Use of Cu, Ni and Co Metal Nanoparticles Generated in Acidic Hydrogels as Catalysts in the Reduction of Nitro Phenols. *Journal of Hydrogels*, *1*(1), 63-69.

[22] Wang, Tian, Dezhang Ren, Zhibao Huo, Zhiyuan Song, Fangming Jin, Mingwei Chen, and Luyang Chen. "A nanoporous nickel catalyst for selective hydrogenation of carbonates into formic acid in water." *Green Chemistry* 19, no. 3 (2017): 716-721.

[23] C. Kresge, M. Leonowicz, W. Roth, J. Vartuli, J. Beck. Ordered mesoporous molecular sieves synthesized by a liquid-crystal template mechanism. Nature 359, 710 (1992).

[24] You, B., Zhang, Y., Yin, P., Jiang, D., Sun, Y., 2018. Universal molecular-confined synthesis of interconnected porous metal oxides-N-C frameworks for electrocatalytic water splitting. Nano Energy 48, 600–606.

[25] Zhao, D., Liu, X.-H., Guo, J.-H., Xu, H.-J., Zhao, Y., Lu, Y., Sun, W.-Y., 2018. Porous Metal–Organic Frameworks with Chelating Multiamine Sites for Selective Adsorption and Chemical Conversion of Carbon Dioxide. Inorg. Chem. 57, 2695–2704.

[26] Wachsman, E.D., Bishop, S.R., 2018. Porous ceramic molten metal composite solid oxide fuel cell anode. US10044057B2.

[27] Padilla, A. P., Rodríguez, J. A., & Saitúa, H. A. (1997). Synthesis and water ultrafiltration properties of silver membrane supported on porous ceramics. *Desalination*, *114*(3), 203-208.

[28] Song, F.-Z., Zhu, Q.-L., Yang, X., Zhan, W.-W., Pachfule, P., Tsumori, N., Xu, Q., 2018. Metal–Organic Framework Templated Porous Carbon-Metal Oxide/Reduced Graphene Oxide as Superior Support of Bimetallic Nanoparticles for Efficient Hydrogen Generation from Formic Acid. Advanced Energy Materials 8, 1701416.

[29] Li, Q., Zhu, S., & Lu, Y. (2017). 3D porous Cu current collector/Li-metal composite anode for stable lithium-metal batteries. *Advanced Functional Materials*, *27*(18), 1606422.

[30] Rolison, D. R., & Dunn, B. (2001). Electrically conductive oxide aerogels: new materials in electrochemistry. *Journal of Materials Chemistry*, *11*(4), 963-980.

[31] Busch, P. A., Cheston, S. P., & Greywall, D. S. (1984). Properties of sintered-silver heat exchangers. *Cryogenics*, *24*(8), 445-447.

[32] Walsh, D., Arcelli, L., Ikoma, T., Tanaka, J., & Mann, S. (2003). Dextran templating for the synthesis of metallic and metal oxide sponges. *Nature materials*, *2*(6), 386.

[33] Liang, S., Li, Y., Chen, Y., Yang, J., Zhu, T., Zhu, D., ... & Zhou, X. (2017). Liquid metal sponges for mechanically durable, all-soft, electrical conductors. *Journal of Materials Chemistry C*, *5*(7), 1586-1590.

[34] Mann, S., & Ozin, G. A. (1996). Synthesis of inorganic materials with complex form. *Nature*, *382*(6589), 313.

[35] Reuss, G, Disteldorf, W.,Grundler, O.& Hilt, A. in *Ullman's Encyclopedia of Industrial Chemistry* 6th edn Vol. 15 1–34 (Wiley-VCH, Weinheim, 2002).

[36] Li, C., Iqbal, M., Lin, J., Luo, X., Jiang, B., Malgras, V., Wu, K.C.-W., Kim, J., Yamauchi, Y., 2018. Electrochemical Deposition: An Advanced Approach for Templated Synthesis of Nanoporous Metal Architectures. Acc. Chem. Res. 51, 1764–1773.

[37] Krishna, K. S., Sandeep, C. S., Philip, R., & Eswaramoorthy, M. (2010). Mixing does the magic: a rapid synthesis of high surface area noble metal nanosponges showing broadband nonlinear optical response. *ACS nano*, *4*(5), 2681-2688.

[38] Deka, P., Deka, R. C., & Bharali, P. (2014). In situ generated copper nanoparticle catalyzed reduction of 4-nitrophenol. *New Journal of Chemistry*, *38*(4), 1789-1793.

[39] Nabil, B., Morshed, M. N., Nemeshwaree, B., Christine, C., Julien, V., Olivier, T., & Abdelkrim, A. (2019). Development of new multifunctional filter based nonwovens for organics

pollutants reduction and detoxification: High catalytic and antibacterial activities. *Chemical Engineering Journal*, *356*, 702-716.

[40] Islam, M. T., Dominguez, N., Ahsan, M. A., Dominguez-Cisneros, H., Zuniga, P., Alvarez, P. J., & Noveron, J. C. (2017). Sodium rhodizonate induced formation of gold nanoparticles supported on cellulose fibers for catalytic reduction of 4-nitrophenol and organic dyes. *Journal of environmental chemical engineering*, *5*(5), 4185-4193.

[41] Islam, M. T., Saenz-Arana, R., Wang, H., Bernal, R., & Noveron, J. C. (2018). Green synthesis of gold, silver, platinum, and palladium nanoparticles reduced and stabilized by sodium rhodizonate and their catalytic reduction of 4-nitrophenol and methyl orange. *New Journal of Chemistry*, *42*(8), 6472-6478.

[42] Nemanashi, M.; Meijboom, R. Synthesis and characterization of Cu, Ag and Au dendrimer-encapsulated nanoparticles and their application in the reduction of 4-nitrophenol to 4-aminophenol. J. Colloid Interf. Sci. 2013, 389, 260-267.

[43] Islam M. T.; Padilla J. E.; Dominguez N.; Alvarado D. C.; Alam M. S.; Cooke P.; Tecklenburg M. M. J.; Noveron J. C. Green synthesis of gold nanoparticles reduced and stabilized by squaric acid and supported on cellulose fibers for the catalytic reduction of 4-nitrophenol in water. RSC Adv. 2016, 94, 91185-91191.

[44] Wang, C., O'Connell, M. J., & Chan, C. K. (2015). Facile one-pot synthesis of highly porous carbon foams for high-performance supercapacitors using template-free direct pyrolysis. *ACS applied materials & interfaces*, *7*(16), 8952-8960.

[45] Ye, K., Ma, X., Huang, X., Zhang, D., Cheng, K., Wang, G., & Cao, D. (2016). The optimal design of Co catalyst morphology on a three-dimensional carbon sponge with low cost, inducing better sodium borohydride electrooxidation activity. *RSC Advances*, *6*(47), 41608-41617.

[46] Singh, A., Shirolkar, M., Limaye, M. V., Gokhale, S., Khan-Malek, C., & Kulkarni, S. K. (2013). A magnetic nano-composite soft polymeric membrane. *Microsystem technologies*, *19*(3), 409-418.

[47] Ali, B., Tasirin, S., Aminayi, P., Yaakob, Z., Ali, N., & Noori, W. (2018). Non-Supported Nickel-Based Coral Sponge-Like Porous Magnetic Alloys for Catalytic Production of Syngas and Carbon Bio-Nanofilaments via a Biogas Decomposition Approach. *Nanomaterials*, *8*(12), 1053.

[48] Shenoy, U. S., & Shetty, A. N. (2014). Simple glucose reduction route for one-step synthesis of copper nanofluids. *Applied Nanoscience*, *4*(1), 47-54.

[49] Patterson, A. L. The Scherrer formula for X-ray particle size determination. Phys. Rev. 1939, 56, 978−982.

[50] Verma, S., & Dutta, R. K. (2017). Enhanced ROS generation by ZnO-ammonia modified graphene oxide nanocomposites for photocatalytic degradation of trypan blue dye and 4-nitrophenol. *Journal of environmental chemical engineering*, *5*(5), 4776-4787.

[51] Baxter, R. J., & Hu, P. (2002). Insight into why the Langmuir–Hinshelwood mechanism is generally preferred. *The Journal of chemical physics*, *116*(11), 4379-4381.

[52] Islam, M. T., Hernandez, C., Ahsan, M. A., Pardo, A., Wang, H., & Noveron, J. C. (2017). Sulfonated resorcinol-formaldehyde microspheres as high-capacity regenerable adsorbent for the removal of organic dyes from water. *Journal of environmental chemical engineering*, *5*(5), 5270-5279.

[53] Ajmal, M., Siddiq, M., Al-Lohedan, H., & Sahiner, N. (2014). Highly versatile p (MAc)–M (M: Cu, Co, Ni) microgel composite catalyst for individual and simultaneous catalytic reduction of nitro compounds and dyes. *RSC Advances*, *4*(103), 59562-59570.

[54] Sahiner, N., Sagbas, S., & Aktas, N. (2015). Very fast catalytic reduction of 4-nitrophenol, methylene blue and eosin Y in natural waters using green chemistry: p (tannic acid)–Cu ionic liquid composites. *RSC Advances*, *5*(24), 18183-18195.

[55] Zhang, Y.; Zhu, P.; Chen, L.; Li, G.; Zhou, F.; Lu, D. D.; Sun, R.; Zhou, F.; Wong, C. P. Hierarchical Architectures Of Monodisperse Porous Cu Microspheres: Synthesis, Growth Mechanism, HighEfficiency and Recyclable Catalytic Performance. J. Mater. Chem. A 2014, 2, 11966−11973.

[56] Li, X. Z.; Wu, K. L.; Ye, Y.; Wei, X. W. Controllable Synthesis of Ni Nanotube Arrays and Their Structure-dependent Catalytic Activity toward Dye Degradation. CrystEngComm 2014, 16, 4406−4413.

[57] Veerakumar, P., Chen, S. M., Madhu, R., Veeramani, V., Hung, C. T., & Liu, S. B. (2015). Nickel nanoparticle-decorated porous carbons for highly active catalytic reduction of organic dyes and sensitive detection of Hg (II) ions. *ACS applied materials & interfaces*, *7*(44), 24810-24821.

[58] Ajmal, M., Demirci, S., Siddiq, M., Aktas, N., & Sahiner, N. (2016). Simultaneous catalytic degradation/reduction of multiple organic compounds by modifiable p (methacrylic acid-co-acrylonitrile)–M (M: Cu, Co) microgel catalyst composites. *New Journal of Chemistry*, *40*(2), 1485-1496.

Graphical abstract

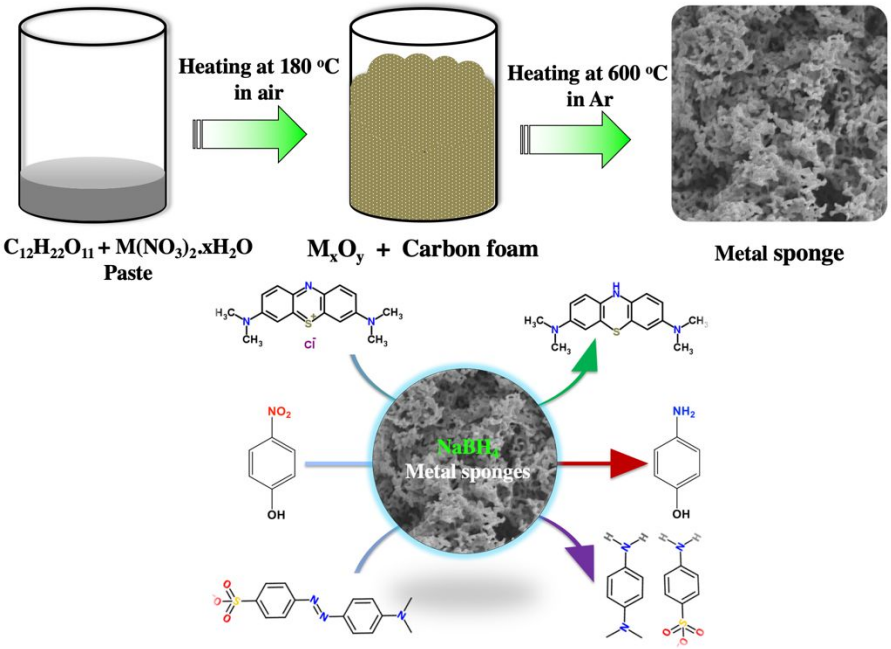

Facile synthesis of cobalt, nickel, and copper sponges and their catalytic properties for the reduction of 4-nitrophenol, methyl orange, and methylene blue.